JACS
JOURNAL OF THE AMERICAN CHEMICAL SOCIETY

Article

pubs.acs.org/JACS

Dual Stress and Thermally Driven Mechanical Properties of the Same Organic Crystal: 2,6-Dichlorobenzylidene-4-fluoro-3-nitroaniline

Soumyajit Ghosh, Manish Kumar Mishra, Somnath Ganguly, and Gautam R. Desiraju*

Solid State and Structural Chemistry Unit, Indian Institute of Science, Bangalore 560 012, India

Supporting Information

ABSTRACT: An elastic organic crystal, 2,6-dichlorobenzylidine-4-fluoro-3-nitroaniline (DFNA), which also shows thermosalient behavior, is studied. The presence of these two distinct properties in the same crystal is unusual and unprecedented because they follow respectively from isotropy and anisotropy in the crystal packing. Therefore, while both properties lead from the crystal structure, the mechanisms for bending and thermosalience are quite independent of one another. Crystals of the low-temperature (α) form of the title compound are bent easily without any signs of fracture with the application of deforming stress, and this bending is within the elastic limit. The crystal structure of the α-form was determined ($P2_1/c$, $Z = 4$, $a = 3.927(7)$ Å, $b = 21.98(4)$ Å, $c = 15.32(3)$ Å). There is an irreversible phase transition at 138 °C of this form to the high-temperature β-form followed by melting at 140 °C. Variable-temperature X-ray powder diffraction was used to investigate the structural changes across the phase transition and, along with an FTIR study, establishes the structure of the β-form. A possible rationale for strain build-up is given. Thermosalient behavior arises from anisotropic changes in the three unit cell parameters across the phase transition, notably an increase in the b axis parameter from 21.98 to 22.30 Å. A rationale is provided for the existence of both elasticity and thermosalience in the same crystal. FTIR studies across the phase transition reveal important mechanistic insights: (i) increased $\pi\cdots\pi$ repulsions along [100] lead to expansion along the a axis; (ii) change in alignment of C−Cl and NO_2 groups result from density changes; and (iii) competition between short-range repulsive ($\pi\cdots\pi$) interactions and long-range attractive dipolar interactions (C−Cl and NO_2) could lie at the origin of the existence of two distinctive properties.

1. INTRODUCTION

The study of the mechanical properties of molecular solids as a function of their crystal structures is a very active branch of crystal engineering today.[1−3] Gross mechanical motion may be conveniently considered as a basis for understanding actuation of organic and metal−organic solids from the molecular to the macroscopic level. Materials that show mechanical motion under the influence of different external stimuli such as pressure, heat, and light are becoming candidates for self-actuating devices.[4−11] Such substances have a wide array of applications as high-performance smart materials, for example, as artificial muscles, biomimetics, and technomimetics.[8,9,12−17] These applications result from their restorative capabilities and stress dissipating behavior. Recent research has uncovered several crystalline systems that show different responses when they are subjected to external stimuli.[8,18−28] These durable and resilient compounds are becoming increasingly important; their highly ordered structures can sustain efficient charge transport. However, the design of such solids, in which rapid and reversible macroscopic shape changes are enabled through collective molecular perturbations, remains a challenge. Thermosalient crystals have attracted attention owing to their potential sensing and actuating behavior.[29−34] Thermosalient behavior occurs during a phase transformation, and there are small yet distinctly anisotropic changes in the crystallographic unit cell parameters across the phase transition. The overall packing in the two phases is usually the same in terms of symmetry and space group, but the phase transitions are associated with fast, rapid release of accumulated strain energy.[32−37] In order that one might obtain a deeper insight into the relevant structure−property relationships, the structural changes need to be investigated. For example, Panda et al. studied colossal positive and negative thermal expansion in a pentamorphic organometallic martensite.[32] Sahoo et al. conducted a detailed study of structure-kinematic aspects of the self-actuation behavior of a thermosalient crystal.[29] This has been attributed to first-order displacive solid−solid transition that occurs with Bain distortion.[38−41]

Elastic properties in molecular solids are largely determined by the isotropy of crystal packing.[8,18] Recent studies by Ghosh and Reddy on caffeine co-crystals have established that bending of elastic organic crystals is related to isotropic packing with the presence of relatively weak and dispersive interactions in all directions.[8] In a more general study, we have systematically

Received: May 22, 2015
Published: July 20, 2015

DOI: 10.1021/jacs.5b05324
J. Am. Chem. Soc. 2015, 137, 9912−9921

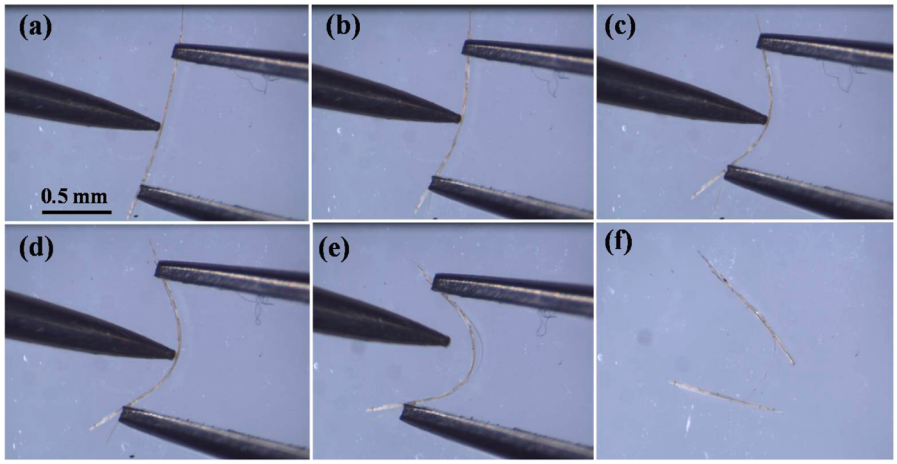

Figure 1. Snapshots (a) through (f) show stepwise elastic bending of DFNA crystal and shape recovery after breakage.

designed seven halogenated *N*-benzylideneanilines (Schiff bases) using the techniques of crystal engineering[1,2] and found common underlying structural features which lead to high flexibility and elasticity (structures of these seven compounds are given in the Supporting Information S1).[18]

Incorporating two mechanical properties in the same organic crystal is a difficult task but may have futuristic applications in devices that respond to two different external stimuli. In this paper, we discuss the results of studies on a serendipitously discovered elastic organic crystal that also shows thermosalient behavior. The occurrence of these two properties, elasticity, and thermosalient behavior in the same crystal seems to be a contradiction in terms because elasticity follows from isotropic packing, while thermosalient behavior requires some degree of anisotropy in the crystal packing. The demonstration of different mechanical properties under the influence of two distinct external stimuli is therefore quite exceptional and is unprecedented. The present study is an attempt to rationalize elastic bending and the thermosalient phase transition in the same crystal, 2,6-dichlorobenzylidine-4-fluoro-3-nitroaniline (DFNA). This compound is also a Schiff base and belongs to the same chemical class as the seven compounds we studied previously.[18] To what extent are the structural requirements for these two properties in DFNA independent of each other? To obtain some clarity on these matters, a number of methods ranging from microscopy, X-ray diffraction to FTIR spectroscopy were used. Optical microscopy provides evidence of the elastic behavior, while single crystal X-ray diffraction (SCXRD) studies afford a rationale for the same. On the other hand, hot stage microscopy, variable-temperature powder X-ray diffraction (VTPXRD) and FTIR allowed clear insights into the thermosalient phase transition. The results obtained from all these studies point to mechanisms that underlie the two distinct macroscopic phenomena in this system.

2. RESULTS AND DISCUSSION

2.1. Elastic Bendable Property. Slender, acicular crystals of DFNA (obtained by slow evaporation of MeOH solutions containing 1 equiv each of 2,6-dichlorobenzaldehyde and 4-fluoro-3-nitroaniline) were used to study the elastic properties. These crystals are orange colored and of 4−6 mm in length and 0.02−0.04 mm in thickness and show growth along the *a* axis. When the crystals were held with a pair of forceps and force applied from opposite ends with a needle, they could be bent easily without any signs of fracture (see Video 1 in the Supporting Information). This process was found to be reversible as the crystal straightens out immediately upon withdrawal of the force.[8,18,42,43] This sequence could be repeated many times indicating the fatigueless nature of the crystal as well as its restorative character. Figure 1 clearly shows that the crystal can be easily bent into a curve with the help of needles and forceps, but when bent beyond a threshold limit, the crystal breaks into two pieces, each of which recover their original shape confirming once again the restorative character of these changes in the DFNA crystal.

2.1.1. SCXRD Study. To understand the structural basis for elastic bending, we carried out the single crystal structure determination of DFNA. The crystal packing is similar to our previous series of elastic crystals and the title compound here belongs to the same chemical class.[18] The compound crystallizes in the monoclinic space group $P2_1/c$ with one molecule in the asymmetric unit (Supporting Information S2). The aromatic rings are puckered in a *trans* conformation across the CH═N bond. Individual molecules are connected via weak C−H···F (3.907 Å, 3.133 Å, 141.91°) interactions to form zigzag tapes along the *b* axis. Neighboring tapes are further connected via multiple interactions such as type I Cl···Cl (3.369 Å, $\theta_1 = \theta_2 = 152.35°$), type II F···Cl (3.177 Å, $\theta_1 = 131.9°$, $\theta_2 = 172.73°$), and C−H···O (2.645 Å, 132.39°; 2.719 Å, 133.83°) hydrogen bonds to form corrugated sheets parallel to the (100) plane shown in Figure 2. The molecules in each tape form $\pi\cdots\pi$ stacks parallel to the *a* axis resulting in 2D corrugated sheets parallel to the (001) plane. The overall packing is isotropic in that all the weakly dispersive interactions are energetically comparable (1−3 kcal mol^{-1}).[43] This feature is critical to the elastic behavior of molecular solids.

2.1.2. Structural Basis of Elastic Bendable Property. We have shown earlier that elasticity in this family of Schiff bases is due to a criss-cross arrangement of molecules.[18] In DFNA, these molecules can be envisaged as forming a tape structure (Figure 2). The neighboring tapes further interlock to form 2D sheets. The title compound behaves in a manner largely similar to those studied earlier by us with respect to its elastic bendable property.[18] In order that one may understand the structural basis of bending we performed face indexing of a long needle shaped crystal (Supporting Information S3). It was found that two pairs of side faces (011)/(0−1−1) and (0−11)/(01−1) are bendable and the top face is (−101) as given in Figure 3.

DOI: 10.1021/jacs.5b05324
J. Am. Chem. Soc. 2015, 137, 9912−9921

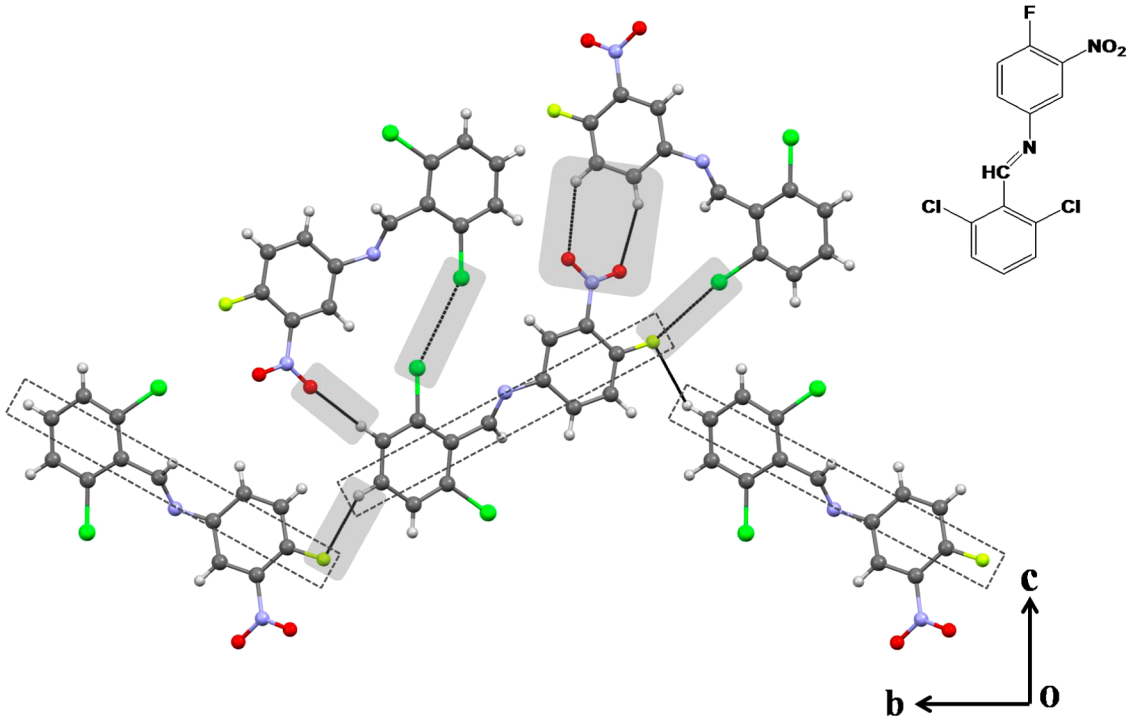

Figure 2. Crystal packing of DFNA down [100]. Hydrogen- and halogen-bond supramolecular synthons are shaded in gray. Note the C−H···O heterodimer, type I Cl···Cl, type II F···Cl, and C−H···F patterns. The criss-cross arrangement of molecules is depicted as three rectangular boxes with dashed lines.

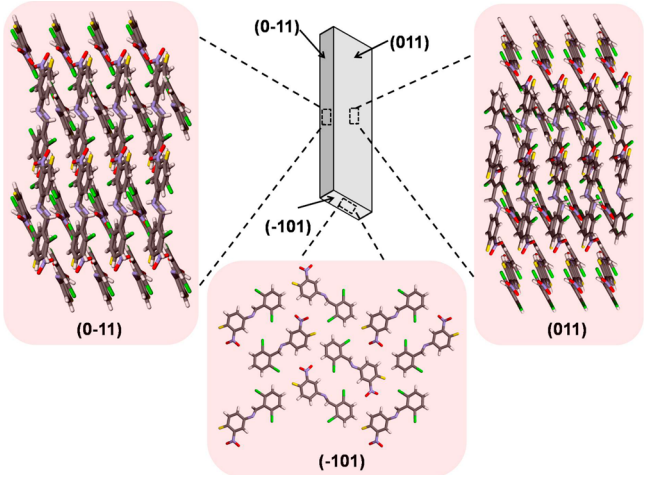

Figure 3. Crystal morphology and packing in DFNA. The views from both bendable side faces (0−11) and (011) show the corrugation which prevents long-range sliding of molecules during bending.

The molecules form $\pi\cdots\pi$ stacks along the *a* axis, and a criss-cross packing with corrugation angle ~70° is evident from the bendable side faces. This packing induces a spring-like behavior inside the crystal. Multiple halogen interactions such as Cl···Cl, F···Cl, and also C−H···O hydrogen bonds are observed and behave as "structural buffers" during bending.[43−46] These interactions can be ruptured or restored easily during bending giving rise to elastic behavior, but as the crystal packing is isotropic and interlocked, it prevents easy slippage of molecules thereby blocking irreversible plastic deformation. Because the molecules are connected to form zigzag tapes, long-range molecular motion is restricted. It may be noted that during bending, the torsion angle changes allow the molecules to move away slightly from their equilibrium positions. Because the crystal quickly reverts back to its original position when the stress is removed, it is clear that the energy barrier for this movement is minimal.

As might have been expected, the $\pi\cdots\pi$ stacking in DFNA is along the needle axis. In the bent state, the $\pi\cdots\pi$ separation would increase in the outer arc with the molecules becoming less inclined to each other (Figure 4). A change in torsion angle causes the molecules to distribute strain energy uniformly in the

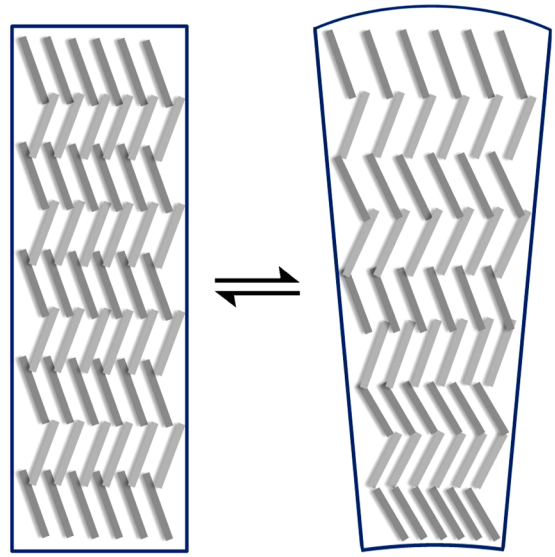

Figure 4. Schematic representation of molecular rearrangement in DFNA during bending. In the outer arc, the $\pi\cdots\pi$ distance increases, while in the inner arc, the molecules are compressed with the $\pi\cdots\pi$ distance decreasing.

DOI: 10.1021/jacs.5b05324
J. Am. Chem. Soc. 2015, 137, 9912−9921

outer arc. In the inner arc, the intermolecular separations decrease accompanied by a compression of molecules resulting in greater corrugation. Molecules located in the middle of the crystal are virtually unaffected. Figure 4 shows that molecules in the outer and inner peripheries are strained to a greater or lesser extent. Thus, coordinated short-range molecular movement of individual molecules gets magnified into macroscopic elastic bending. When the applied force exceeds a threshold limit, the structure becomes strained leading to crystal breakage. The threshold limit was found to depend upon the crystal thickness, and greater bending was generally achieved with thinner crystals. The restoring ability of several weak interactions such as Cl···Cl, F···Cl and C−H···O can cause the crystal to pull the molecules back to their original positions in a spring-like fashion. Therefore, it is clear that a number of weak and dispersive interactions in the corrugated isotropic structure are vital in imparting elastic behavior.[8,18,43]

Interesting as these elastic properties are, they are shared by the title compound DFNA with a number of chemically related benzylidene anilines.[18] What is quite distinctive about DFNA is its thermosalience, a feature not shared with other benzylidene anilines we studied. Accordingly, we set about a more detailed study of this second property not only from the structural viewpoint but also from a spectroscopic one, with FTIR as the method of choice, so that mechanistic insights might be obtained from the spectrospic changes across the martensitic phase transition.

2.2. Thermosalient Behavior. *2.2.1. Hot Stage Microscopy.* When subjected to heating, the DFNA crystal shows thermosalient behavior wherein the crystals undergo macroscopic motility followed by melting (see Video 2). Two types of effects were observed: (i) elastic bending and (ii) crystal splitting along the needle axis. DSC performed on single crystals showed a small endotherm at 138 °C followed by the melting endotherm at 140 °C. This phase transition is irreversible as is evidenced from heating−cooling experiments (Figure 5). As the lifetime of the new phase is small,

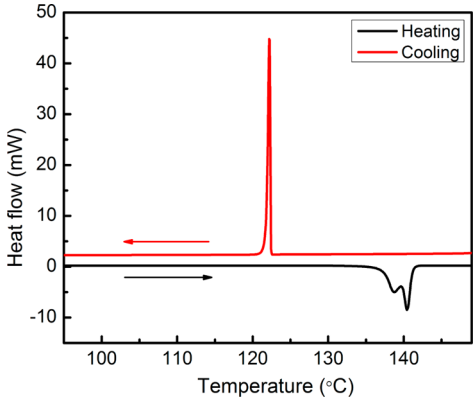

Figure 5. DSC heating−cooling shows martensitic phase transition $\alpha \rightarrow \beta$ just before melting. The cooling exotherm shows that the phase transformation is irreversible.

macroscopic resilience is observed only for a short duration before the onset of melting. We refer to the low- and high-temperature phases of DFNA as α and β henceforth.

While attempting to collect hot stage microscopy data, it was consistently observed that the crystals split along the needle axis followed by a scissoring motion of the broken parts due to continued heating (Figures 6 and 7). The small temperature

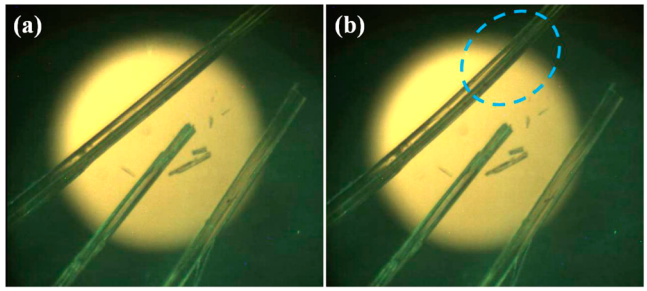

Figure 6. Crystal bends prior to splitting (note area within blue dashed ellipse).

window between the phase transition and the melting temperature indicates that the phase transition is associated with abrupt molecular motion with new molecular orientations in the martensite phase.[41,47−52] The new structure leads to accumulated strain energy which is subsequently released at an interface leading to splitting. Further heating causes the broken parts to undergo scissoring motion after which the crystal melts. Strain energy in the crystal is developed due to a rapid anisotropic expansion along a preferred direction. This $\alpha \rightarrow \beta$ martensitic transition is a first-order displacive, diffusionless phase transition.[53] Although the structural change is minimal, its diffusionless and cooperative nature causes a sudden buildup of strain energy. Since the temperature range of the martensitic phase is small, it was not possible to probe deeper into the dynamics of the phase transition, with calorimetry.

2.2.2. Expansion of Cell Axes from SCXRD Study. From a variable-temperature SCXRD study, trends were obtained regarding the *a*, *b*, and *c* axes expansions. Data were collected at −175, − 125, − 75, − 25, and 25 °C (Table 1). It was noted that while the *a* axis increases by 3.45%, the *b* and *c* axes increase only by 1.9% and 1.18% over this temperature range. The unit cell volume was found to increase by 6.47%. Since the *a* axis expansion is greater than the *b* and *c* axes, it was concluded that the $\pi\cdots\pi$ distance increases at a faster rate than the other interactions.[54]

Figure 8 also suggests that increasing Cl···Cl, F···Cl, and O···H distances (Supporting Information S4) are due to intertape separation. This ultimately leads to a slightly greater *b* axis expansion (1.9%) compared to *c* axis expansion (1.19%). There is also a consistent increase in the C−H···F distance. Our initial hypothesis was that this trend would continue into the β-phase. However, our VTPXRD observations proved to be different, and it was found that *b* axis expansion is more significant during the phase transition and takes place with shrinkage of the *c* axis.

2.2.3. VTPXRD. A VTPXRD study was carried out to investigate the structural changes occurring across the phase transition. Data were recorded from room temperature to 140 °C (Figure 9). At 138 °C, premelting was noticed along with onset of the martensitic phase β. Rietveld refinement method for PXRD patterns was done to rationalize the *a*, *b*, and *c* axes expansions. It was noted that the peaks shifted toward lower 2θ with increasing temperature, which is in line with *a* and *b* axes expansion.

The kinematic behavior of the phase transition may be explained in two steps. The first is an initial bending. The second is crystal splitting. Bending is caused by a thermal gradient which arises because molecules adjacent to the hot surface of the HSM get extended, while those located in the interior

DOI: 10.1021/jacs.5b05324
J. Am. Chem. Soc. 2015, 137, 9912−9921

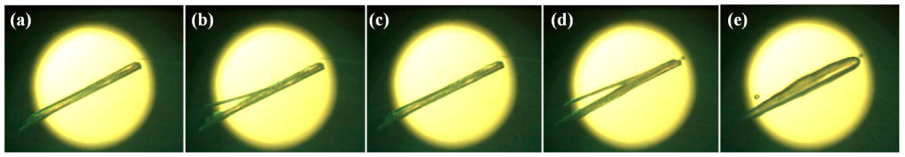

Figure 7. DFNA crystal splitting during the phase transition.

Table 1. Unit Cell Parameters for DFNA Crystal From −175 to 25 °C

temp (°C)	a (Å)	b (Å)	c (Å)	β (°)	V (Å^3)
−175	3.796(9)	21.57(5)	15.14(3)	100.77(5)	1218(5)
−125	3.850(3)	21.798(19)	15.282(14)	101.06(2)	1258.7(19)
−75	3.8719(14)	21.799(8)	15.258(5)	101.374(18)	1262.5(8)
−25	3.877(7)	21.79(4)	15.21(3)	101.82(4)	1258(4)
25	3.927(7)	21.98(4)	15.32(3)	101.32(4)	1297(4)

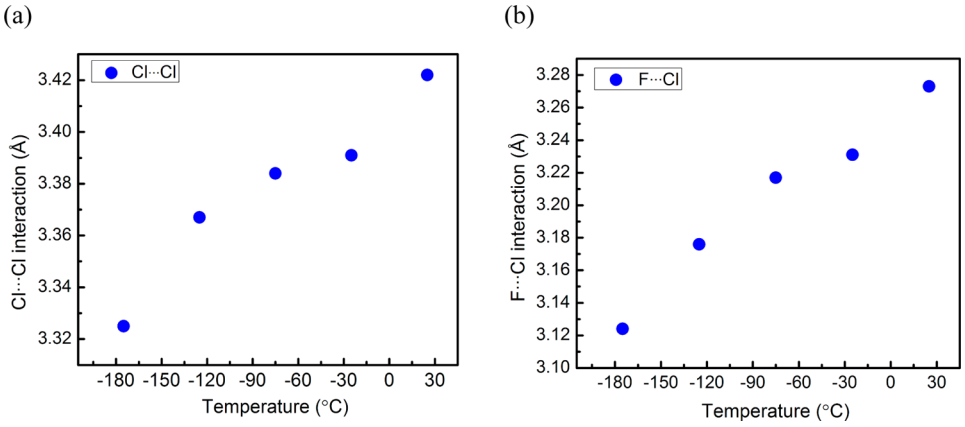

Figure 8. Cl···Cl and F···Cl distances as a function of temperature from −175 to 25 °C indicate the increasing tape separations along the c axis.

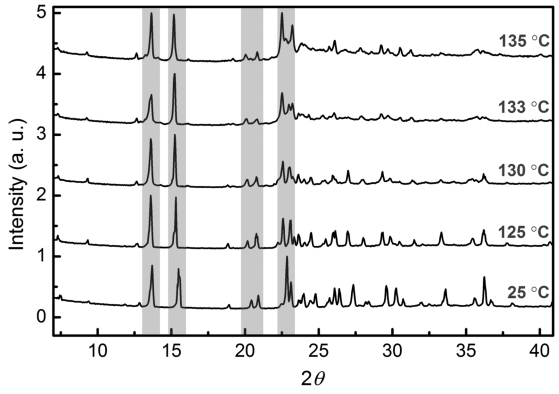

Figure 9. Variable-temperature PXRD from room temperature to 135 °C showing continuous shift of major peaks toward lower 2θ indicating a and b axis expansion.

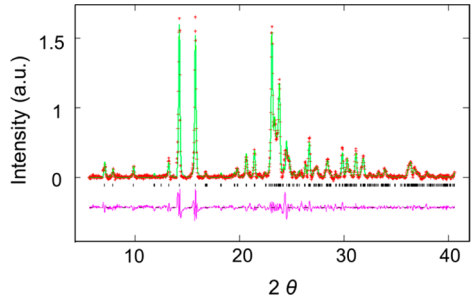

Figure 10. Rietveld refinement for PXRD at 135 °C was carried out. Observed (red daggers), calculated (lime green lines) and difference (pink lines) profiles are shown. The vertical bars (black) indicates Bragg reflections. R_p, R_{wp} and χ^2 are 1.16, 1.50, and 1.06, respectively, confirming the good fit of the PXRD pattern.

remain relatively unaffected. This leads to curving of the crystal reminiscent of a bimetallic strip. In a little while, however, the crystal straightens out presumably because some kind of thermal equilibration has taken place. As the a axis expansion is the highest we see bending along (011) in the first step. However, in the second step, namely phase transition, there is just that degree of structural anisotropy created in the crystal that results in a thermosalient effect with breakage of the crystal. Rietveld refinement was carried out for the PXRD pattern obtained at 135 °C (Figure 10). The packing of the two phases is almost the same although changes are seen in the a, b, and c axes lengths in the thermosalient β-phase (Table 2). There is an expansion along the a (5.88%) and b (1.5%) axes that is offset by shrinkage in the c axis (−2.5%). The splitting of the crystal is attributed to preferential anisotropic cell expansion along the b axis. Positive thermal expansion along the b axis (+1.5%) and negative thermal expansion along the c axis (−2.5%) trigger self-actuation and motility.[55−59] Expansion along the b axis is not easily dissipated by the relatively smaller number of molecules in that direction. Therefore, the crystal reacts to released strain energy at the interface, and this has an adverse effect on its integrity. As the crystal lattice is not extensively hydrogen bonded, it is unable to absorb the accumulated strain energy developed and dissipate it sufficiently quickly. This effectively translates into thermosalient behavior.

DOI: 10.1021/jacs.5b05324
J. Am. Chem. Soc. 2015, 137, 9912−9921

Table 2. Unit Cell Parameters of DFNA at Different Temperatures during the Thermosalient Transition

phase	a (Å)	b (Å)	c (Å)	β (°)	V (Å^3)
25 °C	3.927(7)	21.98(4)	15.32(3)	101.32(4)	1297(4)
135 °C	4.158(2)	22.3091(26)	14.922(23)	95.7(9)	1378(9)
Δ/%	+5.88	+1.5	−2.5	−5.54	+6.27
138 °C	4.156(9)	22.494(9)	14.963(9)	95.47(9)	1392.39
Δ/%	+5.83	+2.33	−2.33	−5.77	+7.38

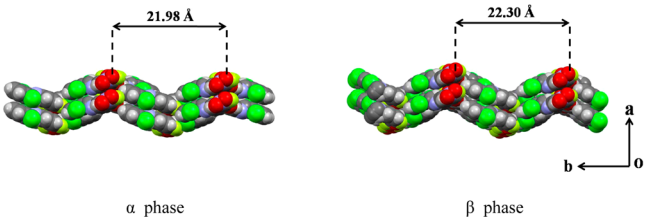

Figure 11. Structural view (space filling model) of phases α and β. Note the expansion along the b axis.

Structurally speaking, the difference between the α- and β-phases is illustrated in Figure 11. At the molecular level, there is no significant conformational difference. The absence of incongruity among the two phases indicates overall macroscopic integrity in the system. The extent of corrugation also does not vary too much in the two structures, suggesting conservation of the main packing features. The main cause of the thermosalient effect is the expansion along the b axis (Figure 11) in association with a concomitant increase in tape separation along the a axis and mutual approach between the tapes along the c axis.

2.2.4. Effect of Grinding. In order to understand whether the new phase can be categorized as the thermodynamically stable form, we checked PXRD of the room temperature phase (α-form) before and after grinding and compared this with the simulated pattern. It was noted that even after sustained grinding for 30 min, the α-form does not convert into β (Supporting Information S5). This means that this martensitic transformation is not kinetically governed. It can be achieved only upon heating and this is manifested by the impressive self-actuation.

2.2.5. Variable-Temperature FTIR Studies. In addition to SCXRD and PXRD, a careful variable-temperature FTIR study was done in the region of the transition to ascertain the nature of the martensitic phase β. The intensity, widths, and frequency shifts of major bands were studied in an attempt to derive a possible molecular mechanism of the martensitic phase transition. An explicit idea of relative orientation of molecules and intertape separation which take place in the new phase was obtained. Spectra were recorded in the 4000−500 cm^{-1} region at temperatures between 135 and 141 °C at 1 °C intervals. FTIR frequencies and intensities of aromatic C−H stretch, C−Cl stretch, and ν_{asym} NO_2 stretching modes were monitored through the phase transition.

2.2.5.1. Frequency Variations. Figure 12a shows the aromatic C−H stretching band in the FTIR spectra of the crystal through the martensitic phase transition at 139 °C, while Figure 13a shows the plot of the frequency of the band against temperature. The band blueshifts with an increase in temperature and flattens out at the phase transition (Figure 12a). When a phase transition involves pressure, density, or volume changes, IR active internal vibrations exhibit changes due to competition between short-range repulsive blueshifts and long-range attractive redshifts.[60] The blueshifts (collisional repulsions) are due to repulsions between nearest neighbors (Supporting Information S6: expression for repulsive force term).[61] In the present system, blueshifts at the martensitic phase transition are due to repulsions between aromatic groups, and these repulsions are followed by weakening of the $\pi\cdots\pi$ interactions. Such repulsions also cause a axis elongation. Concomitant C−H stretch band broadening at the phase transition indicates increase in vibrational dephasing due to collisions.[62] Figure 12b shows the FTIR spectra of the C−Cl stretching mode at 780 cm^{-1} and the ν_{asym} NO_2 stretching vibration at 1530 cm^{-1} (Supporting Information S7). The bands are seen to redshift at the phase transition (Figure 13b and Supporting Information S8). Such redshifts occur due to long-range attractive interactions that lead to ordering of C−Cl/NO_2 groups from an antiparallel to a parallel orientation. Thus, it can be said that at the phase transition, $\pi\cdots\pi$ repulsions between aromatic molecules occurring along the a axis lead to an expansion of this axis

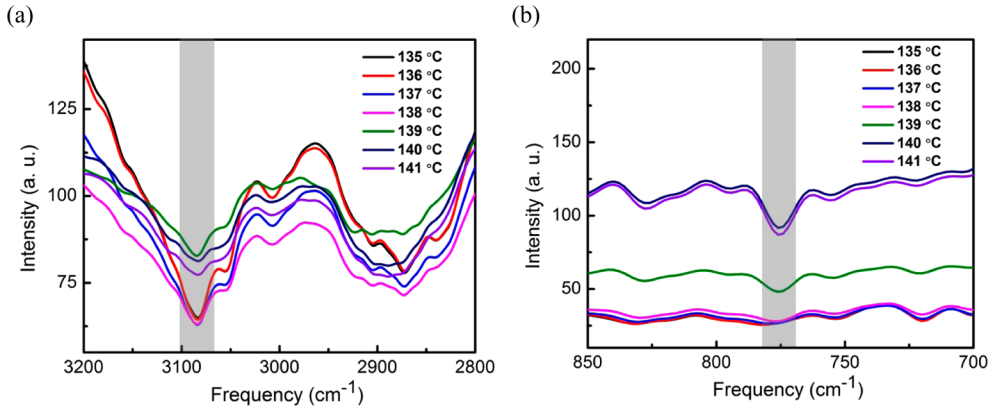

Figure 12. (a) IR spectra of the aromatic C−H stretch (3080 cm^{-1}) through the thermosalient phase transition. (b) IR spectra of the C−Cl stretch (780 cm^{-1}) through the phase transition.

DOI: 10.1021/jacs.5b05324
J. Am. Chem. Soc. 2015, 137, 9912−9921

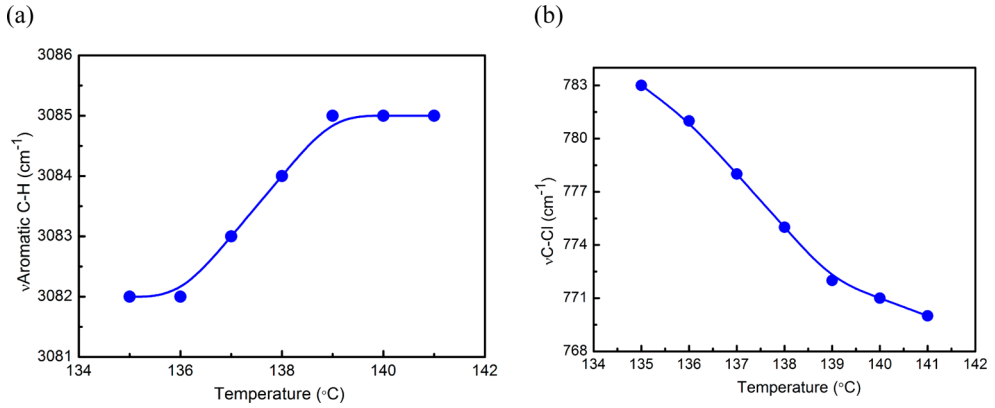

Figure 13. (a) Frequency of the aromatic C−H stretch through the thermosalient phase transition. (b) Frequency of the C−Cl stretch through the phase transition.

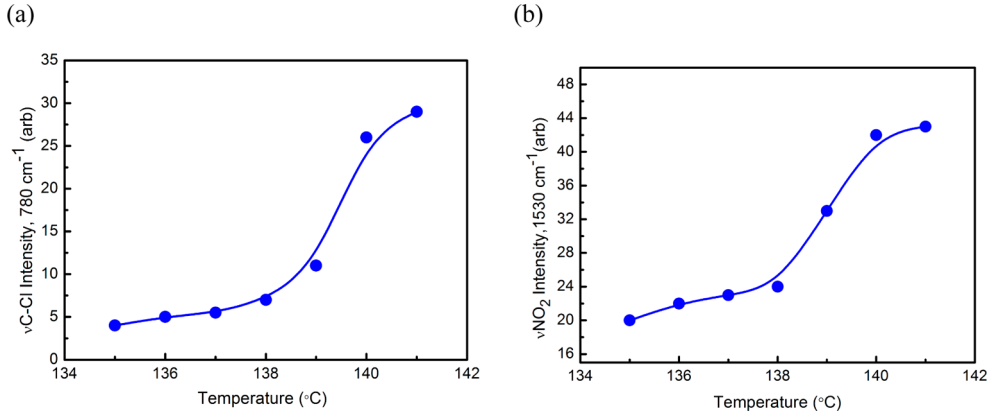

Figure 14. (a) Intensity of the C−Cl stretch through the thermosalient phase transition. (b) Intensity of the $\nu_{as}NO_2$ stretch through the thermosalient phase transition.

and weakened $\pi\cdots\pi$ interactions, while increasing long-range attractive interactions of C−Cl and NO_2 groups result in changes in the *b* and *c* axes.

2.2.5.2. Intensity Variations. The intensities of the C−Cl stretch or the ν_{asym} NO_2 stretching vibration increase at the phase transition, indicating that the number of aligned C−Cl bonds is also increased. While the alignment of the C−Cl units increases six times, alignment is more than doubled for the NO_2 stretching vibration (Figure 14a,b). Increase in the C−Cl stretch/NO_2 stretch intensity is due to alignment of the two modes driven by the thermosalient phase transition. Such ordering of dipoles follow from long-range attractive interactions.[63] Alignment of dipoles is known to result in higher intensities of IR bands as in liquid−solid phase transitions.[64] Earlier studies on the liquid → solid β → solid α phase transition of acetonitrile have shown alignment of dipoles change from antiparallel to parallel alignment due to such long-range ordering.[65] The changes of the C−Cl/NO_2 stretching bands in the present study are similar indicating that the phase transition is accompanied by ordering of dipoles and long-range attractive interactions (Figure 14b and Supporting Information S9: expression for dipole moment). A small narrowing of the bands indicates ordering and reduction in disorder, collisions, and dephasing. Attractive interactions may also arise between aromatic groups and the C−Cl/NO_2 groups or between aligned dipoles. Whether the alignment leads to changes in the *c* axis is not clear and would need more detailed investigations on similar crystal systems. FTIR spectra recorded at 145 °C show further broadening of the aromatic C−H stretch and are indicative of increased repulsions and vibrational dephasing. The spectra do not indicate any broadening or intensity drop of the C−Cl/NO_2 stretches at 145 °C that would indicate a molten isotropic phase with orientational disorder. This strongly suggests absence of melting (orientational and vibrational disorder) and the presence of a "memory" of the martensitic phase beyond the melting temperature.[66,67] (The C−Cl stretch at 145 °C is shown in Supporting Information S10). A depiction of the phase transition as evinced from the FTIR study is shown in Figure 15.

In our previous study of elastic crystals[18] it was shown that elasticity arises from a criss-cross packing of molecular tapes in isotropic structures with energetically comparable halogen

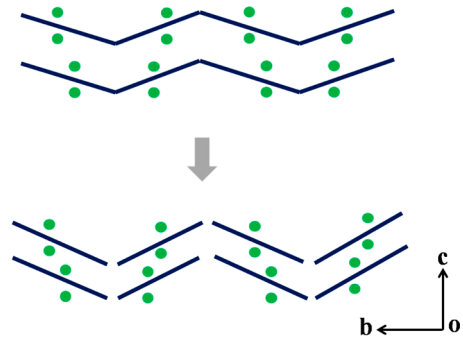

Figure 15. Schematic of zigzag tape of molecules in DFNA to show *b* axis expansion and *c* axis compression in phase β.

DOI: 10.1021/jacs.5b05324
J. Am. Chem. Soc. 2015, 137, 9912−9921

bonds (Cl···Cl or Cl···Br). In such elastic crystals, criss-cross arrangement of neighboring tapes prevents easy slippage and allows molecular movement only to short distances from thermodynamic lattice positions. To identify the origin of the additional mechanical (thermosalient) property in the same DFNA crystals, we tried to understand the reasons for *anisotropy in a largely isotropic structure*. We conjectured that an anisotropy of the type observed could have arisen due to the introduction of fluoro and nitro groups previously absent. The anisotropy would then be caused by directional dipole−dipole interactions (Cl···F, Cl···Cl) and C−H···O hydrogen-bond interactions.[68−70] This is well corroborated by the FTIR study that indicates competitive repulsive $\pi\cdots\pi$ interactions in one direction and long-range attractive dipolar interactions (C−Cl and NO_2) in an orthogonal direction. To summarize, the dual properties seen in the present crystalline system require some degree of anisotropic character in an otherwise isotropic crystal structure with the mechanisms of each property being independent of the other. Isotropy with criss-cross packing leads to elastic behavior, while anisotropy with competitive interactions drives the thermosalient property. A combined consideration of crystallographic and spectroscopic aspects leads to a clearer understanding of these phenomena.

3. CONCLUSIONS

Our studies identify dual mechanical properties in the same crystal, namely pressure-induced elastic mechanical bending and temperature-induced crystal splitting. These distinct mechanical manifestations have been attributed to different mechanisms involving strain energy build-up. The two phenomena are independent of each other (at least visually) but may be interconnected through the elastic nature of the crystals. Elastic bending is related to an interlocked, isotropic structure with a multitude of weak and dispersive interactions. Thermosalient behavior is associated with structural anisotropy and manifests itself as crystal splitting. It occurs with an anisotropic expansion of the crystal upon heating. In the title compound, 2,6-dichlorobenzylidene-4-fluoro-3-nitroaniline, strain energy is developed because of expansion of the *b* axis and compression of the *c* axis. The enigmatic feature in the present study is the existence of two properties in the same crystal, each of which follows from seemingly contradistinctive structural features. DFNA is similar to seven other Schiff bases in its elastic behavior and one can conclude that its crystal packing is similarly isotropic to these previously studied seven compounds (structures given in the Supporting Information S1).[18] However, none of these seven compounds exhibit thermosalient behavior. Therefore, there is some degree of anisotropic character in the structure of the low temperature form α of DFNA which is not present in the seven other halogenated derivatives studied previously. It is this anisotropy that triggers the martensitic phase transformation to the β-form that leads then to thermosalient behavior. This anisotropy could follow from the C−H···O or C−H···F interactions[68,69] that are largely absent in the seven other compounds studied earlier,[18] because they do not contain nitro and fluoro groups. One could say that DFNA is the most anisotropic among a series of isotropic crystal structures. VTPXRD studies on the system taken with the FTIR study point to the fact that in the martensitic phase transition, the main interactions are affected unequally; some are strengthened, while others are weakened. Considering also that the two properties of interest are affected by these different sets of interactions, this could be a reason why two properties are even observed.

4. EXPERIMENTAL SECTION

4.1. Materials. All the compounds were purchased from Sigma-Aldrich. Commercially available solvents were used as received without further purification.

4.2. Single Crystal Preparation. Long, acicular crystals of the elastic bendable crystal DFNA were prepared by adding 1 equiv each of the corresponding 2,6-dichlorobenzaldehyde and 4-fluoro-3-nitroaniline in hot MeOH followed by slow evaporation of the solution at ambient conditions. The crystals were obtained after 3−4 days.

4.3. SCXRD. Single crystal X-ray diffraction data were collected on a Rigaku Mercury 375/M CCD (XtaLAB mini) diffractometer using graphite monochromated Mo Kα radiation at 25, −25, −75, −125, and −175 °C. The data were processed with the Rigaku CrystalClear software.[71] Structure solution and refinements were executed using SHELX97[72] using the WinGX3 suite[73] of programs. Refinement of coordinates and anisotropic thermal parameters of non-hydrogen atoms were performed with the full-matrix least-squares method. Positions of the hydrogen atoms were located either from difference Fourier map or calculated using the riding model. Crystallographic cif files (CCDC nos. 1050261−1050265) are available at www.ccdc.cam.ac.uk/data_request/cif or as part of the Supporting Information S2.

4.4. VTPXRD. Variable-temperature powder X-ray diffraction patterns were recorded using Philips analytical (PAN Analytical) X-ray BV diffractometer (Netherlands) using Cu Kα (1.5418 Å) as the X-ray source. Spectra were recorded at different temperature, ranging from 125 to 140 °C and from 5° to 90° with 2°/min rate at 45 kV and 30 mA using 1/2° divergence slit and 1° antiscatter slit in "Anton Paar TTK 450 (*z*-axis) + LNC" stage mode. The samples were prepared as powder on low background chromium-plated Cu holder (0.2 mm depth and 10 mm × 14 mm area) with Pt 100 sensor.

4.4.1. Analysis of Crystal Packing. Rietveld refinement was done on PXRD pattern obtained at 135 and 138 °C. The structure was obtained at 135 °C. R_p, R_{wp}, and χ^2 are 1.16, 1.50, and 1.06, respectively, indicating good fitting of PXRD pattern. Similarity index (Π) was calculated between room temperature (25 °C) and 135 °C. It is defined as

$$\prod = \left| \frac{a + b + c}{a' + b' + c'} \right| - 1 \cong 0$$

4.5. DSC. DSC was recorded on a Mettler Toledo DSC 823e instrument. For the high-temperature study, DFNA crystals were heated within a range from 25 to 150 °C with a step size of 2 °C/min. Similarly for low-temperature study, the cooling rate was 2 °C/min within a range from 150 to 25 °C in inert nitrogen atmosphere.

4.6. Hot Stage Microscopy. The thermo-microscopic behavior of DFNA crystals was performed on a Wagner & Munz hot stage microscope from 50 °C until melting. The video 3 was recorded simultaneously during the heating process.

4.7. Variable-Temperature FTIR. Solid-state variable-temperature FTIR spectra of the DFNA crystals were recorded on a PerkinElmer frontier FTIR spectrometer in an ATR mode. The FTIR spectrometer was equipped with a heating/cooling stage from Specac. Samples were scanned from 4000 to 600 cm^{-1} at a resolution of ±2 cm^{-1} from temperatures ranging from 25 to 141 °C. In the range 135 to 141 °C, samples were heated at 1 °C temperature interval and spectra recorded at each degree elevation.

■ ASSOCIATED CONTENT

Supporting Information

The Supporting Information is available free of charge on the ACS Publications website at DOI: 10.1021/jacs.5b05324.

Crystallographic information table, PXRD, face index image of crystal, variable-temperature IR spectra, and supplementary figures (PDF)

Crystallographic information (CIF)

Videos of elastic and thermosalient behavior of the DFNA crystal (AVI)

DOI: 10.1021/jacs.5b05324
J. Am. Chem. Soc. 2015, 137, 9912−9921

AUTHOR INFORMATION

Corresponding Author

*desiraju@sscu.iisc.ernet.in

Notes

The authors declare no competing financial interest.

ACKNOWLEDGMENTS

S.Ghosh thanks DST for a Young Scientist Fellowship. M.K.M. thanks CSIR for a Senior Research Fellowship. S. Ganguly is grateful to IISc for a Project Assistantship. G.R.D. thanks the Department of Science and Technology, India for a J. C. Bose Fellowship. The authors thank Ms. Debdyuti Mukherjee and Prof. S. Sampath for the VTPXRD of the samples. We thank Mr. Sourav Laha (SSCU) for helping with the Rietveld refinement of the PXRD patterns.

REFERENCES

(1) Desiraju, G. R. *J. Am. Chem. Soc.* **2013**, *135*, 9952.
(2) Desiraju, G. R.; Vittal, J. J.; Ramanan, A. *Crystal Engineering: A Text Book*; World Scientific: Singapore, 2011.
(3) Varughese, S.; Kiran, M. S. R. N.; Ramamurty, U.; Desiraju, G. R. *Angew. Chem., Int. Ed.* **2013**, *52*, 2701.
(4) Balzani, V. V.; Credi, A.; Raymo, F. M.; Stoddart, J. F. *Angew. Chem., Int. Ed.* **2000**, *39*, 3348.
(5) Browne, W. R.; Feringa, B. L. *Nat. Nanotechnol.* **2006**, *1*, 25.
(6) Terao, F.; Morimoto, M.; Irie, M. *Angew. Chem., Int. Ed.* **2012**, *51*, 901.
(7) Kobatke, S.; Takami, S.; Muto, H.; Ishikawa, T.; Irie, M. *Nature* **2007**, *446*, 778.
(8) Ghosh, S.; Reddy, C. M. *Angew. Chem., Int. Ed.* **2012**, *51*, 10319.
(9) Burgert, I.; Fratzl, P. *Philos. Trans. R. Soc., A* **2009**, *367*, 1541.
(10) Fletcher, S. P.; Dumur, F.; Pollard, M. M.; Feringa, B. L. *Science* **2005**, *310*, 80.
(11) Garcia-Garibay, M. A. *Proc. Natl. Acad. Sci. U. S. A.* **2005**, *102*, 10771.
(12) Fratzl, P.; Barth, F. G. *Nature* **2009**, *462*, 442.
(13) Lv, S.; Dudek, D. M.; Cao, Y.; Balmurali, M. M.; Gosline, J.; Li, H. *Nature* **2010**, *465*, 69.
(14) Morimoto, M.; Irie, M. *J. Am. Chem. Soc.* **2010**, *132*, 14172.
(15) Koshima, H.; Takechi, K.; Uchimoto, H.; Shiro, M.; Hashizume, D. *Chem. Commun.* **2011**, *47*, 11423.
(16) Koshima, H.; Ojima, N.; Uchimoto, H. *J. Am. Chem. Soc.* **2009**, *131*, 6890.
(17) Kellermayer, M. S.; Smith, S. B.; Granzier, H. L.; Bustamante, C. *Science* **1997**, *276*, 1112.
(18) Ghosh, S.; Mishra, M. K.; Kadambi, S. B.; Ramamurty, U.; Desiraju, G. R. *Angew. Chem., Int. Ed.* **2015**, *54*, 2674.
(19) Panda, M. K.; Ghosh, S.; Yasuda, N.; Moriwaki, T.; Mukherjee, G. D.; Reddy, C. M.; Naumov, P. *Nat. Chem.* **2015**, *7*, 65.
(20) Naumov, P.; Sahoo, S. C.; Zakharov, B. A.; Boldyreva, E. V. *Angew. Chem., Int. Ed.* **2013**, *52*, 9990.
(21) Reddy, C. M.; Kirchner, M. T.; Gundakaram, R. C.; Desiraju, G. R. *Chem. - Eur. J.* **2006**, *12*, 2222.
(22) Reddy, C. M.; Krishna, G. R.; Ghosh, S. *CrystEngComm* **2010**, *12*, 2296.
(23) Nath, N. K.; Pejov, L.; Nichols, S. M.; Hu, C.; Saleh, N.; Kahr, B.; Naumov, P. *J. Am. Chem. Soc.* **2014**, *136*, 2757.
(24) Reddy, C. M.; Gundakaram, R. C.; Basavoju, S.; Kirchner, M. T.; Padmanabhan, K. A.; Desiraju, G. R. *Chem. Commun.* **2005**, 3945.
(25) Reddy, C. M.; Padmanabhan, K. A.; Desiraju, G. R. *Cryst. Growth Des.* **2006**, *6*, 2720.
(26) Zhu, L.; Al-Kaysi, R. O.; Bardeen, C. J. *J. Am. Chem. Soc.* **2011**, *133*, 12569.
(27) Shtukenberg, A. G.; Punin, Y. O.; Gujral, A.; Kahr, B. *Angew. Chem., Int. Ed.* **2014**, *53*, 672.
(28) Naumov, P.; Kowalik, J.; Solntsev, K. M.; Baldridge, A.; Moon, J. S.; Kranz, C.; Tolbert, L. M. *J. Am. Chem. Soc.* **2010**, *132*, 5845.
(29) Sahoo, S. C.; Panda, M. K.; Nath, N. K.; Naumov, P. *J. Am. Chem. Soc.* **2013**, *135*, 12241.
(30) Skoko, Ž.; Zamir, S.; Naumov, P.; Bernstein, J. *J. Am. Chem. Soc.* **2010**, *132*, 14191.
(31) Shima, T.; Muraoka, T.; Hoshino, N.; Akutagawa, T.; Kobayashi, Y.; Kinbara, K. *Angew. Chem., Int. Ed.* **2014**, *53*, 7173.
(32) Panda, M. K.; Runčevski, T.; Sahoo, S. C.; Belik, A. A.; Nath, N. K.; Dinnebier, R. E.; Naumov, P. *Nat. Commun.* **2014**, *5*, 4811.
(33) Sahoo, S. C.; Sinha, S. B.; Kiran, M. S. R. N.; Ramamurty, U.; Dericioglu, A. F.; Reddy, C. M.; Naumov, P. *J. Am. Chem. Soc.* **2013**, *135*, 13843.
(34) Panda, M. K.; Runčevski, T.; Husain, A.; Dinnebier, R. E.; Naumov, P. *J. Am. Chem. Soc.* **2015**, *137*, 1895.
(35) Horie, M.; Suzaki, Y.; Hashizume, D.; Abe, T.; Wu, T.; Sassa, T.; Hosokai, T.; Osakada, K. *J. Am. Chem. Soc.* **2012**, *134*, 17932.
(36) Horie, M.; Sassa, T.; Hashizume, D.; Suzaki, Y.; Osakada, K.; Wada, T. *Angew. Chem., Int. Ed.* **2007**, *46*, 4983.
(37) Etter, M. C.; Siedle, A. R. *J. Am. Chem. Soc.* **1983**, *105*, 641.
(38) Centore, R.; Jazbinsek, M.; Tuzi, A.; Roviello, A.; Capobianco, A.; Peluso, A. *CrystEngComm* **2012**, *14*, 2645.
(39) Zamir, S.; Bernstein, J.; Greenwood, D. *Mol. Cryst. Liq. Cryst. Sci. Technol., Sect. A* **1994**, *242*, 193.
(40) Ding, J.; Herbst, R.; Praefcke, K.; Kohne, B.; Saenger, W. *Acta Crystallogr., Sect. B: Struct. Sci.* **1991**, *47*, 739.
(41) Wu, H.; Reeves-McLaren, N.; Pokorny, J.; Yarwood, J.; West, A. R. *Cryst. Growth Des.* **2010**, *10*, 3141.
(42) Chen, C. T.; Ghosh, S.; Reddy, C. M.; Buehler, M. J. *Phys. Chem. Chem. Phys.* **2014**, *16*, 13165.
(43) Mukherjee, A.; Desiraju, G. R. *IUCrJ* **2014**, *1*, 49.
(44) Metrangolo, P.; Neukirch, H.; Pilati, T.; Resnati, G. *Acc. Chem. Res.* **2005**, *38*, 386.
(45) Priimagi, A.; Cavallo, G.; Metrangolo, P.; Resnati, G. *Acc. Chem. Res.* **2013**, *46*, 2686.
(46) Mukherjee, A.; Tothadi, S.; Desiraju, G. R. *Acc. Chem. Res.* **2014**, *47*, 2514.
(47) Wu, H.; West, A. R. *Cryst. Growth Des.* **2011**, *11*, 3366.
(48) Kaneko, F.; Yano, J.; Tsujiuchi, H.; Tashiro, K. *J. Phys. Chem. B* **1998**, *102*, 327.
(49) Smallman, R. E. *Modern Physical Metallurgy*, 3rd ed.; Butterworth: London, 1970.
(50) Haasen, P. *Physical Metallurgy*; Cambridge University Press: Cambridge, U.K., 1996.
(51) Roitburd, A. L. *Mater. Sci. Eng., A* **1990**, *127*, 229.
(52) Roitburd, A. L.; Kurdjumov, G. V. *Mater. Sci. Eng.* **1979**, *39*, 141.
(53) Krumhansl, J. A.; Yamada, Y. *Mater. Sci. Eng., A* **1990**, *127*, 167.
(54) Since the crystal faces are not coaxial with *a*, *b*, and *c* as such, the description of structures in terms of orthogonalized cell might, rigorously speaking, be more effective. However, the difference in the β angle between the original monoclinic cell and the orthogonalized cell is just 11.32°. From this it is clear that a representation in the orthogonalized cell would lead to practically the same conclusions with respect to structural arguments concerning alignment of faces (Supporting Information S11).
(55) Krishnan, R. S.; Srinivasan, R.; Devnarayanan, S. *Thermal Expansion of Crystals*; Pergamon: Oxford, 1979.
(56) Birkedal, H.; Schwarzenbach, D.; Pattison, P. *Angew. Chem., Int. Ed.* **2002**, *41*, 754.
(57) Goodwin, A. L.; Kepert, C. *Phys. Rev. B: Condens. Matter Mater. Phys.* **2005**, *71*, 140301.
(58) Yang, C.; Wang, X.; Omary, M. A. *Angew. Chem., Int. Ed.* **2009**, *48*, 2500.
(59) Das, D.; Jacobs, T.; Barbour, L. J. *Nat. Mater.* **2010**, *9*, 36.
(60) Schweizer, K. S.; Chandler, D. *J. Chem. Phys.* **1982**, *76*, 2296.
(61) Ellis, A.; Zehentbauer, F. M.; Kiefer, J. *Phys. Chem. Chem. Phys.* **2013**, *15*, 1093.
(62) Oxtoby, D. W. *J. Chem. Phys.* **1979**, *70*, 2605.
(63) Schweizer, K. S.; Chandler, D. *J. Chem. Phys.* **1982**, *76*, 2296.
(64) Thomas, M.; Brehm, M.; Fligg, R.; Vohringer, P.; Kirchnerw, B. *Phys. Chem. Chem. Phys.* **2013**, *15*, 6608.

DOI: 10.1021/jacs.5b05324
J. Am. Chem. Soc. 2015, 137, 9912−9921

(65) Abramczyk, H.; Paradowska-Moszkowska, K. *Chem. Phys.* **2001**, *265*, 177.
(66) Ubbelohde, A. R. *The Molten State of Matter: Melting and Crystal Structure*; John Wiley: Chichester,1978.
(67) The melting entropy of a non-spherical and rigid molecular system can be expressed by a positional and orientational entropy term as below:[66]

$$S_m = S_{pos} + S_{orient} + \text{other terms}$$

where S_m is the total melting entropy, S_{pos} is the positional/vibrational entropy term, and S_{orient} is the orientational entropy term. Orientational entropy is not rotational entropy but entropy of orientational-randomization. For spherical molecular crystals, the entropy increases for the S_{orient} may be considerably greater than S_{pos}.
(68) Thalladi, V. R.; Weiss, H.-C.; Bläser, D.; Boese, R.; Nangia, A.; Desiraju, G. R. *J. Am. Chem. Soc.* **1998**, *120*, 8702.
(69) Desiraju, G. R.; Steiner, T. *The Weak Hydrogen Bond in Structural Chemistry and Biology*; Oxford University Press: Oxford, 1999.
(70) The formation of a C−H···O or C−H···F bond at 138 °C was difficult to see in the FTIR spectra as phase transition driven C−H band broadening and blueshifting start at this temperature and could mask a C−H shift or intensity change on formation of the bond.
(71) Rigaku Mercury375R/M CCD. *Crystal Clear-SM Expert 2.0* rc14; Rigaku Corporation: Tokyo, 2009.
(72) Sheldrick, G. M. *Acta Crystallogr., Sect. A: Found. Crystallogr.* **2008**, *64*, 112.
(73) Farrugia, L. J. *J. Appl. Crystallogr.* **1999**, *32*, 837.

DOI: 10.1021/jacs.5b05324
J. Am. Chem. Soc. 2015, 137, 9912−9921